OXFORD GENETICS

GENETICS, 2024, iyae130
https://doi.org/10.1093/genetics/iyae130
Advance Access Publication Date: 3 September 2024
Investigation

Transcriptomic analysis of meiotic genes during the mitosis-to-meiosis transition in *Drosophila* females

Ana Maria Vallés,[1,†] Thomas Rubin ,[1,†] Nicolas Macaisne ,[1,3] Laurine Dal Toe,[1,4] Anahi Molla-Herman,[1] Christophe Antoniewski ,[2] Jean-René Huynh [1,*]

[1]Center for Interdisciplinary Research in Biology, Collège de France, Université PSL, CNRS, INSERM, 75005 Paris, France
[2]ARTbio Bioinformatics Analysis Facility, IBPS, CNRS, Sorbonne Université, Institut Français de Bioinformatique, 75005 Paris, France
[3]Present address: Institut Jacques Monod, Université Paris Cité, CNRS, 75013 Paris, France
[4]Present address: CBS (Centre de Biologie Structurale), Univ Montpellier, CNRS, INSERM, Montpellier, France

*Corresponding author: Center for Interdisciplinary Research in Biology, Collège de France, Université PSL, CNRS, INSERM, 75005 Paris, France. Email: jean-rene.huynh@college-de-france.fr
[†]These authors contributed equally to this work.

Germline cells produce gametes, which are specialized cells essential for sexual reproduction. Germline cells first amplify through several rounds of mitosis before switching to the meiotic program, which requires specific sets of proteins for DNA recombination, chromosome pairing, and segregation. Surprisingly, we previously found that some proteins of the synaptonemal complex, a prophase I meiotic structure, are already expressed and required in the mitotic region of *Drosophila* females. Here, to assess if additional meiotic genes were expressed earlier than expected, we isolated mitotic and meiotic cell populations to compare their RNA content. Our transcriptomic analysis reveals that all known meiosis I genes are already expressed in the mitotic region; however, only some of them are translated. As a case study, we focused on *mei-W68*, the *Drosophila* homolog of *Spo11*, to assess its expression at both the mRNA and protein levels and used different mutant alleles to assay for a premeiotic function. We could not detect any functional role for Mei-W68 during homologous chromosome pairing in dividing germ cells. Our study paves the way for further functional analysis of meiotic genes expressed in the mitotic region.

Keywords: germline; oocyte; Spo11; recombination; cell cycle; development

Introduction

In organisms reproducing sexually, germline cells produce oocytes and sperms as gametes. Germline cell differentiation starts by an amplification phase through mitosis to increase their numbers and create a pool of precursor cells (Cinalli *et al.* 2008). They then switch to meiosis, which comprises 2 rounds of nuclear divisions to produce haploid gametes. Meiosis is specific to germline cells and requires the expression of unique molecular machineries to pair, recombine, and segregate homologous chromosomes. How germline cells switch from a mitotic to a meiotic program is not fully understood.

Meiosis starts by an extended prophase I during which homologous chromosomes have to find each other in the nuclear space to pair (Bhalla and Dernburg 2008; Zickler and Kleckner 2015). Once homologous chromosomes are paired, their association is stabilized by the synaptonemal complex (SC), the proteinaceous structure that holds homologous axes together (synapsis) and promotes genetic recombination (Cahoon and Hawley 2016). Recombination starts by the formation of developmentally programmed double-strand breaks (DSBs), which can be later repaired as crossovers. Meiotic DSBs are induced by the topoisomerase-like Spo11, which is conserved in all species (Keeney *et al.* 1997; de Massy 2013). These chromosome exchanges create physical links called chiasmata, which keep homologs paired until they orient toward opposite poles of the spindle. This period is subdivided in 5 classical stages (leptotene, zygotene, pachytene, diplotene, and diakinesis) based on chromosome morphologies. The initiation of the pairing process has been defined at the early zygotene stage in *Saccharomyces cerevisiae* (Tsubouchi and Roeder 2005) and at the leptotene stage in *Caenorhabditis elegans* (Crittenden *et al.* 2006; Rohozkova *et al.* 2019), zebrafish (Blokhina *et al.* 2019), and mice (Ishiguro *et al.* 2014; Scherthan *et al.* 2014), by fluorescence in situ hybridization (FISH) analysis and chromosome axis protein imaging. Moreover, chromosome movements, forces, and molecular players that promote pairing have been well characterized by live imaging microscopy in these species (Rubin *et al.* 2020; Kim *et al.* 2022).

However, we and others have found that homologous chromosomes start to pair through centromeres and euchromatic loci during the mitotic phases preceding leptotene in both *Drosophila* males and females (Cahoon and Hawley 2013; Christophorou *et al.* 2013; Joyce *et al.* 2013; Christophorou *et al.* 2015; Rubin *et al.* 2022). Moreover, we showed that this premeiotic pairing requires components of the SC, a structure specific to prophase I of meiosis (Christophorou *et al.* 2013; Rubin *et al.* 2022). Indeed, the C(3)G and Corona proteins, which form the central region of the SC, are transcribed and translated in the mitotic region and localize on one side of the centromeres. It is similar to the initiation of meiosis in

Received on 22 December 2023; accepted on 12 July 2024

budding yeast, where centromeres become "coupled" before meiotic prophase (Tsubouchi and Roeder 2005). This early association also depends on Zip1, a central component of the SC functionally similar to C(3)G in flies and SYCP1 in mice. Furthermore, recent analyses in mice have shown that meiotic genes involved in prophase I are expressed and translated long before the initiation of the meiotic process (Wang *et al.* 2001; Evans *et al.* 2014; Zheng *et al.* 2022). For example, the meiotic cohesin REC8, as in *C. elegans* (Pasierbek *et al.* 2001), and SC proteins are expressed and actively translated in spermatogonia, which go through several mitotic divisions before meiotic entry. In addition, Spo11 protein is also found at very low levels in spermatogonia (Fang *et al.* 2021).

Here, to assess if additional meiotic genes were expressed in the mitotic region of *Drosophila* females, we analyzed the whole genome transcriptome of mitotic and meiotic germline cells.

Material and methods

Flies were maintained on standard medium in 25°C incubators on a 12 h light/dark cycle. Wild-type controls and in combination with additional transgenes of fluorescently tagged proteins were in a w^{1118} background.

Fly stocks and genetics

Fly stocks used in this study are as follows: *bam::GFP/CyO; nos>UASp-RFP::wcd/TM6,Tb* is the full-length *bam* fused to GFP at C-terminus, containing its own promoter and 3′-UTR (Chen and McKearin 2003) and full-length *wicked* fused to red fluorescent protein (RFP) N-terminus, under the control of germline-specific UASp promoter and activated by *nanos-Gal::VP16* (BDSC_4937) (Fichelson *et al.* 2009). To compare *bam::GFP/CyO; nos>UASp-RFP::wcd/TM6,Tb* line to the wild-type white-reference line, we first used Orb as a marker for developmental timing of germline development (Supplementary Fig. 1a and b). We found no difference between the *bam-Bam*::GFP; *nos>wcd*::RFP line and the white-control line. Orb is initially present in all germline cells in early region 1 and 2a, then becomes restricted to the oocyte in region 2b and at the anterior of the oocyte in region 3, and then switches to the posterior of the oocyte in stage 2 egg chambers. We found the 2 lines to be identical. We also analyzed the restriction of the SC to a single cell using an antibody against C(3)G (Supplementary Fig. 1c and d). We found that in region 1 and region 2a, C(3)G was identical in both genetic backgrounds. However, in region 3, we noticed that the SC signal was less intense in the future oocyte in the transgenic line (Supplementary Fig. 1e, "oocyte I"); and at the same time, we observed a stronger signal of C(3)G in the reverting pro-oocyte in the transgenic line (Supplementary Fig. 1d, open arrowhead; Supplementary Fig. 1e, "oocyte II"). Then at stage 2, the transgenic and control lines became identical. These data indicate that there is a transient delay in the restriction of the SC to a single cell in the *bam-Bam::GFP; nos>wcd::RFP line* compared to white flies. We then tested whether this delay could be caused by different number of germline cysts in the germarium, but we found no difference in the number of cysts in region 2 between the two genetic backgrounds (Supplementary Fig. 1f). We also analyzed by RNA FISH whether we could detect differences in gene expression between the 2 lines. We performed RNA FISH for meiotic genes found in RNAseq data, such as *c(3)G*, *Nipped-B*, and *mei-W68* (Supplementary Fig. 3a–c). Quantification of FISH signals in region 2 found no difference in levels of expression of these 3 genes between the transgenic and control lines. Finally, we used a functional assay to test for meiotic differences between these 2 lines, and we measured the occurrence of X chromosome nondisjunction (Supplementary Table 5). In both lines, we found only background frequencies of chromosome nondisjunctions. Overall, our thorough characterization of the *bam-Bam::GFP; nos>wcd::RFP* line revealed only a transient delay in SC restriction to the oocyte. This does not change our transcriptomic analysis of regions 1 and 2.

mei-W68 ^{HA} is a C-terminal 3× HA-linker-6× His-tagged *mei-W68* fly, homozygous viable and subfertile generated by CRISPR/Cas9-mediated Tag knocking strategy (Well Genetics). Catalytic dead *mei-W68* ^{CD} was genome edited at the conserved catalytic domain (Y80F, Y81F) (Romanienko and Camerini-Otero 1999) using the seamless CRISPR/Cas9 strategy (Well Genetics). Flies are homozygous viable and subfertile. *mei-W68*^{1} is a null mutation caused by spontaneous 5 kb TE insertion in exon 2; females have normal SC but show elevated nondisjunction (NDJ) levels (McKim and Hayashi-Hagihara 1998). Df (2R) BSC782/SM6a (BDSC_27354) is a *mei-W68* deficiency, *mei-P22*^{P22} (BDSC_4931). The shRNA lines were as follows: for *white*, P{TRiP.GL00094}attP2 (BDSC_35573); for *C(2)M*, P{TRiP.GL01587}attP2 (BDSC_43977); for *SA*, P{TRiP.GL00534}attP40 (BDSC_36794); for *Nipped-B*, P{ TRiP.GL00574}attP40 (BDSC_36614); and for *sunn*, P{TRiP.HMJ21654} (BDSC_52969). *spn-D*^{2} (BDSC_3326). *y w; RpA-70 EGFP[attP2]* (Blythe and Wieschaus 2015) flies were used to generate lines: *RpA-70 EGFP spn-D*^{2}, *mei-W68*^{1}/CyO; *RpA-70 EGFP spn-D*^{2}, *Df (2R)BSC782/CyO*; and *RpA-70 EGFP spn-D*^{2}*/TM6,tb*.

FACS-sorted germ cells

We used the protocol for isolating mitotic and meiotic cell populations as detailed in Vallés and Huynh (2020). In brief, for each FACS isolation, 800 adult ovaries from *bam::GFP/CyO; nos>UASp-RFP::wcd/TM6,Tb* flies were dissected and collected in complete medium (Schneider's insect medium supplemented with 10% heat-inactivated fetal bovine serum, Sigma-Aldrich), dissociated with elastase at 30°C for 30 min (1 mg/mL, Sigma-Aldrich), and filtered twice (first in 40 µ mesh size, then in 70 µ mesh size, Corning Falcon). Cell suspensions underwent FACS separation (Aria III, BD Biosciences), collecting GFP+ and RFP+ cells and eliminating non-fluorescent cells, clumps, and dead cells. Cells were sorted directly into RNA extraction buffer (ARCTURUS Pico RNA isolation Kit, Applied Biosystems) for purification following the manufacturer's protocol.

Library preparations were done by Fasteris SA (Geneva, Switzerland) using the RNA RiboZero Stranded protocol. Indexed adapters were ligated and multiplexed sequencing performed using Illumina HiSeq 2000 (125 bp single read). At least 2 independent biological samples were prepared for each cell population. Sequences generated by Fasteris were aligned against the *Drosophila melanogaster* reference genome (UCSC dm6) (http://rohsdb.cmb.usc.edu/GBshape/cgi-bin/hgGateway).

qRT-PCR

To validate FACS separations (Fig. 1d), RFP+ and GFP+ sorted cells from *Bam::GFP; nos>Wcd::RFP* ovaries were homogenized with a pestle and RNA extracted using the ARCTURUS PicoPure RNA isolation kit.

To quantify gene expression in *mei-W68*^{1}*/Df (2R) BSC782* flies (Supplementary Fig. 4b), RNA was extracted from 20 pairs of dissected ovaries using the RNeasy Micro Kit (QIAGEN). RNA from w^{1118}ovaries served as control.

For all qRT-PCR reactions, reverse transcription was done using random hexamer oligonucleotides with Superscript III Reverse Transcriptase (Invitrogen) according to the manufacturer's protocol and then by RT-PCR using *Power* SYBR Green© PCR Master Mix (Applied Biosystems). Amplifications were done on a CFX Connect Real-Time PCR machine (Bio-Rad). Two to three biological

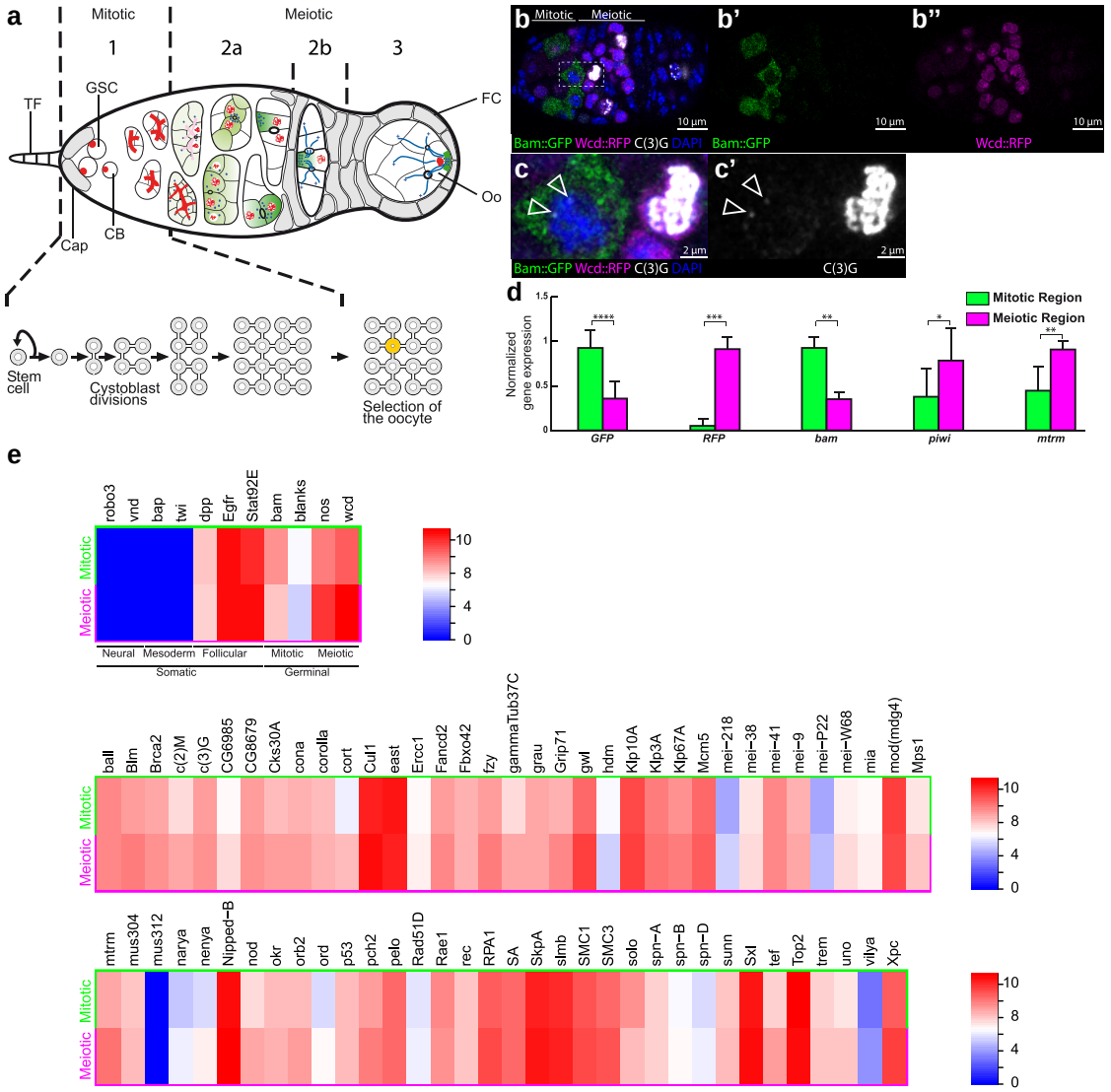

Fig. 1. Meiotic genes are expressed in the mitotic region of the *Drosophila* germarium. a) *Drosophila* germarium depicting the mitotic and meiotic regions. In the anterior part (mitotic zone, also called region 1) at the base of the terminal filament, somatic cap cells surround GSC that divide 4 times giving rise to a 16-cell cyst. GSCs and CBs are marked by the spectrosome (circle) and the developing 2-, 4-, and 8-cell cysts by the fusome (branched structure). After the last mitosis, cysts move to the meiotic zone, subdivided in region 2a, 2b, and 3. Early in region 2a, the SC (thin lines) marks the pro-oocytes with 4 ring canals. By region 2b, the oocyte is selected and is the only cell to remain in meiosis. The follicle cells start to migrate and surround the germline cells as the cyst moves posteriorly to region 3. b–b″) Confocal Z-section of a germarium labeling the mitotic region with Bam::GFP, the meiotic region with Wcd::RFP, the SC with C(3)G, and the cell nuclei with DAPI. c and c′) Magnification of hatched square in b) showing C(3)G nuclear labeling of a cell in the mitotic region (open arrows) adjacent to a SC labeled pro-oocyte. Scale bar: 10 µm in b)–b″); 2 µm in c) and c′). d) RT-PCR gene expression levels of FACS-separated mitotic and meiotic cells using primers to GFP, RFP, *bam*, *piwi*, and *mtrm*. Gene expression levels are defined to 1 relative to the highest value within both population after rp49 normalization. $^{*}P \leq 0.05$, $^{**}P \leq 0.01$, $^{***}P \leq 0.001$, $^{****}P \leq 0.0001$ (Mann–Whitney *U*-test). e) Heatmap of known meiotic genes expressed in FACS-separated Bam::GFP (mitotic) and Wcd::RFP cells (meiotic). In the upper panel are the somatic genes, *robo3* and *vnd* (neural); *bap* and *twi* (mesodermal); *dpp*, *Egfr*, and *Stat92e* (follicle cells), and the sorting controls *bam*, *blanks*, *nos*, and *wcd*. The middle and lower panels represent the heatmap of meiotic genes. Scale represents log2 expression gradient for genes expressed in each of the 2 regions. Notice that neural and mesodermal contaminants are not detected while follicle cells are equally present in both cell populations.

replicates per genotype were used for all qRT-PCR experiments run in triplicate.

Relative expression levels of tested genes were calculated by the C_t method with samples normalized to *rp49* (Schmittgen and Livak, 2008). For each experiment, primer expression in *mei-W68*^{1} was compared to w^{1118} equal 1. To compare gene expression levels between the 2 isolated cell populations, we first normalized each target sample (2–3) with the C_t method (to *rp49*). For each experiment, we then normalized the highest value of the 2 populations to 1. Expression values collected from 3 to 5 experiments were analyzed and transformed into graphs with Prism8 software. Mann–Whitney tests were applied to compare data.

The primers used for the validation of the isolated cell populations were GFP: F 5′AGAGGGCGAATCCAGCTCTGGAG 3′, R 5′CCCAAATCGGCGGTCAGGTGATC 3′; RFP: F 5′ GTCCCCTCAGTT CCAGTACG 30, R 5′ TGTAGATGAACTCGCCGTC 3′; *bam*: F 5′CTGCA TATGATTGGTCTGCACGGC 3′, R 5′CCCAAATCGGCGGTCAGGTG ATC 3′; *piwi*: F 5′ CAGAGGATCTTCATCAGGTG 3′, R 5′ ATCATA TTGGTCACCCCAC 3′; and *mtrm*: F 5′ GAAAGTGCCAACGAAGG TGC 3′, R 5′ CTCCATATTCGAGTCATCCGAAC 3′.

The *mei-W68* primers were A: F 5′ AGCTGCTGCTACTGCTGCTG 3′, R 5′ CCGACTTTTACCGAACGAAAACGAC 3′; B: F 5′ GCTA GAACAATG GATGAATTTTCGG 3′, R 5′ GGAGAGCATGTAAAT CA GCACG 3′; C: F 5′ CGTGCTGATTTACATGCTCTCC 3′, R 5′ GACCGG ACTAGCAGAGGATT 3′; and *rp49*: F 5′ATCTCGCCGCAGTAAACGC 3′, R 5′CCGCTTCAAGGGACAGTATCTG 3′.

Data analysis and heatmap generation

The DESeq2 method for differential analysis of RNAseq data was used (Love *et al.* 2014). As input, we used 3 GFP and 2 RFP distinct biological replicates with counts normalized for differences in sequencing depth using the DESeq normalization tool in Galaxy Mississipi[2] platform (https://mississippi.sorbonne-universite.fr). The normalized raw counts were then used to calculate the base mean for each gene expressed in the mitotic and meiotic cell population to generate the "DESeq2 results extended with base means of conditions" file (Supplementary Table 3). Gene lengths were taken into account by calculating Fragments Per Kilobase Million (FPKM) for each gene (Supplementary Table 4). We then extracted a subset of genes (meiotic, somatic, and separation controls) and obtained Supplementary Table 1 (FPKM in Supplementary Table 2) used for creating a heatmap (Fig. 1e). To generate the heatmap, a list of meiotic genes was compiled from FlyBase Gene Ontology (GO) term (GO: 0007127), excluding genes identified as male-specific and unannotated. Added to the list are known meiotic genes (*SMC1*, *SMC3*, *sunn*, *solo*, and *ord*), *RpA-70*, *dpp*, *egfr*, *Stat9e*, sorting (*bam* and *wcd*), and contamination controls possibly derived from somatic tissues like gut and fat, introduced during dissection of ovaries (*robo3*, *vnd*, *bap*, and *twi*) (see Supplementary Table 1). The resulting values were transformed to log2 and used to generate a heatmap with the heatmap2 tool in the Galaxy Mississipi[2] platform.

Data set repository

Data sets are available from NCBI Sequence Reach Archive under BioProject PRJNA1011850 entitled "Isolation of stage-specific germ cells in *Drosophila* germarium".

Nondisjunction tests

Sex chromosome nondisjunction was monitored by scoring the progeny of *y/BS Y* males mated to females carrying meiotic mutations on the second or third chromosome. For crosses with RNAi lines, the *nanos-Gal::VP16* driver was used. In most cases, a male to female ratio of 5:10 was kept. From these crosses, exceptional diplo-X and nullo-X resulting from sex chromosome nondisjunction and normal gametes are obtained. Frequency of *X* chromosome nondisjunction was calculated as 2(X-ND progeny)/total progeny, where total progeny = [2(X-ND progeny) + (regular progeny) (Gyuricza *et al.* 2016). To determine autosomal 2nd chromosome nondisjunction, females carrying meiotic mutations were mated to *C(2)EN b pr* (BDSC: 1112) males and the number of progeny scored. In most cases, a male to female ratio of 5:10 was kept. From these crosses, only the exceptional diplo-2 and nullo-2 gametes are observed.

Immunohistochemistry

For confocal microscopy, ovaries were dissected in PBS, fixed in 4% paraformaldehyde (PFA)–PBS, and then permeabilized in phosphate buffer Triton (PBT) (0.2% Triton X-100) for 30 min. Samples were incubated overnight with primary antibodies in PBT at 4 °C, washed 4× for 30 min in PBT, and incubated with secondary antibody for 2 h at room temperature, washed 4× for 30 min in PBT. DAPI (1:500) was added during the last wash and then mounted in CityFluor.

For DNA FISH experiments, ovaries were dissected in PBS, fixed in 4% PFA in 1× fix buffer (100 mm potassium cacodylate, 100 mm sucrose, 40 mm sodium acetate, and 10 mm EGTA). Samples were then rinsed 3 times in 2 × SSCT (0.3 M NaCl, 0.03 Na citrate, pH 7.0, 0.1% Tween-20) and incubated with the AACAC and dodeca probes which target the pericentromeric regions of the 2nd and 3rd chromosomes, respectively, as previously described (Christophorou *et al.* 2013). Samples were then rinsed in 2 × SSCT and twice in PBST and processed for immunostaining as described above for confocal microscopy.

For RNA FISH experiments, we followed the HCR in situ hybridization protocol for ovaries as described in Slaidina *et al.* (2021), which was adapted from Choi *et al.* (2018). Custom-designed probes for *mei-W68* (NT_033778), hybridization buffer, wash buffer, and amplification buffer came from Molecular Instruments, Inc.

The following primary antibodies were used: mouse anti-C(3)G 1A8-1G2 (1:500) (gift from S. Hawley, Stowers Institute, USA), rat anti-Cid (1:1,000) (gift from C. E. Sunkel, Universidade do Porto, Portugal), rabbit anti-α-Spectrin (1:1,000 and 1:500 when used with DNA FISH) (gift from R. Dubreuil, University of Chicago, USA), mouse anti-α-Spectrin (1:500, clone 3A9, DSHB), mouse anti-orb (1:500, clone 6H4, DSHB), mouse anti-γH2Av (1:200) (DSHB, UNC93-5.2.1), and rabbit anti-HA-Tag (1:100) (Cell Signaling Technologies, C29A4).

Secondary antibodies conjugated with Cy3 and Cy5 (Jackson laboratories) were used at 1:200, Alexa Fluor Plus 555, and 647 at 1:400 (Thermo Fisher Scientific).

Image acquisition

Ovaries for imaging were taken from 3- to 5-day-old flies. Confocal images of fixed germaria were obtained with a Zeiss LSM 980 NLO confocal microscope except for Supplementary Fig. 1. All images were acquired with a PlanApo 63×/1.4 NA oil objective at 0.5 μm intervals along the z-axis operated by ZEN 2012 software. For Supplementary Fig. 1, confocal images of fixed germaria were taken with a spinning-disk confocal microscope (Yokogawa) operated by Metamorph software on an inverted Nikon Eclipse Ti microscope coupled to a Coolsnap HQ2 camera (Photometrics). All images were acquired with the PlanApo 60×/1.4 NA Oil objective.

Live imaging in oil

Ovaries were dissected in oil (10S, Voltalef, VWR) and transferred onto a coverslip. Germaria were made to stick to the coverslip in oil. All images were acquired on an inverted spinning-disk confocal microscope (Roper/Nikon) operated by Metamorph 7.7 coupled to an sCMOS camera and with a 60×/1.4 oil objective. One Z-stack acquired every 30 s.

Data analysis of images

For quantification of centromere identifier (CID) foci on fixed tissue, we counted the number of distinguishable CID foci within each single nucleus. In all figures, micrographs represent the projections of selected Z-series taken from the first CID foci signal until the last one. For DNA FISH experiments, the 3D distances between the AACAC foci and between the dodeca foci were measured as described (Christophorou *et al.* 2013). Pericentromeric regions of chromosomes were considered as paired when only 1 focus was visible or when 2 foci were separated by a distance less than 0.70 μm and as unpaired when ≥0.70 μm.

Fluorescence intensity measurements of RNA FISH were performed on Z-stack images acquired with identical settings. To define a region of interest (ROI), a Z MAX projection of 3 successive

images within a circle of 50 pixels in diameter was chosen at the center of each analyzed cyst. The cyst stage was determined using the spectrin channel. Cysts located in region 2 were considered as meiotic cysts, while branched cysts of 2-cc, 4-cc, and 8-cc were classified as mitotic cysts. As background control, the ROI was selected in the somatic cells of the nascent stalk before the region 3 cyst of each analyzed germarium. For each cyst and control ROI, the raw integrated density was quantified using Fiji software. The raw data were then transformed into graphs with Prism8 software. Mann–Whitney tests were used to compare fluorescence intensity.

Fluorescence intensity measurements of C(3)G were performed on Z-stack images acquired with identical settings. To define a ROI, a Z MAX projection of 3 successive images within a circle of 50 pixels in diameter was chosen at the center of the C(3)G marked nuclei. The cyst stage was determined using C(3)G staining location in the germarium. As background control, the ROI was selected in the somatic cells of the nascent stalk before the region 3 cyst of each analyzed germarium. For each cyst and control ROI, the raw integrated density was quantified using Fiji software. The raw data were then transformed into graphs with Prism8 software. Mann–Whitney tests were used to compare fluorescence intensity.

Mean cyst number estimations in meiotic region 2 were performed on Z-stack images acquired with identical settings. Cyst boundaries were defined, thanks to α-Spectrin staining, and counted manually.

For the quantification of RPA and H2Av foci on fixed tissues, we counted the number of distinct foci within each individual nucleus. For each channel, the signal was processed using the difference of Gaussians tool available in the GDSC plugin for Fiji. Default threshold was then applied to the resulting stack, generating binary images reconstructed into a 3D stack using the 3D segmentation function of RoiManager3D 4.1.5. The counting of RPA and H2Av dots and the percentage of "overlap" were then calculated using the "Measure 3D" analysis.

Results

Meiotic genes are expressed in the mitotic region

In *Drosophila* females, the processes of mitosis and meiosis occur sequentially throughout the adult life in a structure called the germarium located at the tip of each ovary (Spradling 1993). At the anterior-most part is the mitotic zone, also known as region 1. In this zone, germline stem cells (GSCs) proliferate and self-renew by receiving signals from adjacent somatic tissue that induce the expression of stem cell promoting factors like *nanos*, which mediate the translational repression of differentiation genes (Slaidina and Lehmann 2014). GSCs divide mostly asymmetrically and generate a posterior daughter cell, which differentiates into a precursor cell called cystoblast (CB). The CB undergoes 4 rounds of mitosis, resulting in the formation of a germline cyst consisting of 16 cells (Fig. 1a) (Huynh and St Johnston 2004). During these mitotic divisions, cells remain connected through ring canals and a specialized organelle called the fusome. The branching pattern of the fusome is a useful marker for distinguishing the different stages within the mitotic zone, i.e. GSCs, CBs, and cysts of 2, 4, 8, and 16 cells (de Cuevas and Spradling 1998). The period of rapid synchronized divisions marks the transition phase and the commitment to differentiation. The Bag of marble (Bam) protein induces the differentiation of CBs, and its expression is spatially restricted: suppressed by self-renewal factors in GSCs and activated in CBs and 2-, 4-, and 8-cell cysts (Fig. 1b and c) (Chen and McKearin 2003). After the last mitosis, cysts enter the meiotic zone, also known as region 2a, where all 16 cells that look identical enter meiosis (Carpenter 1975). The presence of the SC in this early meiotic zone marks the initiation of prophase I, with only 2 pro-oocytes progressing to form a complete SC (Hughes *et al.* 2018). At this stage, meiotic DSBs are induced. As the cyst reaches region 2b, only 1 cell within the cyst will become an oocyte, while the remaining 15 cells develop into nurse cells and undergo DNA endoreplication. In this region, the cyst undergoes a significant morphological change, adopting a disk-like shape that is 1-cell thick and spans the entire width of the germarium. Concomitantly, somatic follicle cells begin to migrate and enclose the cyst. As the cyst advances to region 3, also known as stage 1, it assumes a rounded shape forming a sphere. At late pachytene, the oocyte stage is marked with SC and consistently positioned at the posterior pole. Subsequently, the cyst exits the germarium and enters the vitellarium (Huynh and St Johnston 2004).

Although meiosis is described as beginning in early region 2a of the germarium, several proteins needed for homologous chromosomes pairing are already present in mitotically dividing cells of region 1. The SC protein C(3)G is one example, which localizes near the centromeres of chromosomes II and III and whose expression is required for initiating centromeric pairing (Christophorou *et al.* 2013; Fig. 1b and c). To gain a more exhaustive view of the spatiotemporal expression of meiotic genes, we separated the mitotic and meiotic cell populations by FACS and then processed the RNA for high-throughput sequencing. The separation method relied on the restrictive expression pattern and properties of Bam and Wcd transgenic proteins (Vallés and Huynh 2020): Bam::GFP is detectable only in 2–8-cell cysts of region 1 and was used to label the mitotic region (McKearin and Ohlstein 1995). Wcd::RFP has a fast turnover, and when driven by *nanos*-Gal4, it labels a few GSCs and mostly region 2a/b cells; we therefore used it to identify cells in the first stages of meiosis I. The transgenic line (Bam::GFP; nos>Wcd::RFP) labeled germaria and allowed efficient separation of both mitotic and meiotic germ cell population (see Material and Methods section; Supplementary Figs. 1–3; Supplementary Table 5). We confirmed the efficiency of cell sorting by qRT-PCR for specific transcripts. We found that GFP cells were strongly enriched in GFP and *bam* RNA transcripts, while RFP cells were enriched in RFP and *wcd* RNAs (Fig. 1d and e). Endogenous Piwi protein was shown to be strongly downregulated in 2- to 8-cell cysts forming a "piwilesspocket (pilp)" (Dufourt *et al.* 2014). Similarly, we found that *piwi* mRNA levels were lower in the mitotic region compared to the meiotic region (Fig. 1d). *matrimony* (*mtrm*) was reported to be very lowly expressed in the mitotic region and higher in the meiotic region by different methods such as single-cell RNAseq and synchronized germline cells (Slaidina *et al.* 2021; Samuels *et al.* 2024). We confirmed these results by qRT-PCR and RNAseq (Fig. 1d and e; Supplementary Tables 1–4). As an additional control, we used *blanks*, as this gene was previously shown to display the opposite trend with higher expression in mitotic cells than in meiotic cells (Slaidina *et al.* 2021; Samuels *et al.* 2024). Similarly, our results indicate that *blanks* expression levels are higher in the GFP+ cell population than in the RFP+ population (Fig. 1e). To evaluate the contamination by other cell types, we searched for somatic cell markers such as *Robo3* and *vnd* (neural cell), *twist* and *bap* (mesoderm), and *dpp*, *egfr*, and *STAT92*, which are expressed in somatic cells in the germarium but not germline cells. We found that *Robo3*, *vnd*, *twist*, and *bap* RNAs were absent from both cell populations; however, we found that *dpp*, *egfr*, and *Stat92E* were equally present in GFP+ and RFP+ cells (Fig. 1e; Supplementary Tables 1 and 2). These results indicated that there was no contamination by neural or mesodermal tissues, but that some ovarian somatic cells were equally present in both isolated cell populations. Despite the presence of somatic cells in

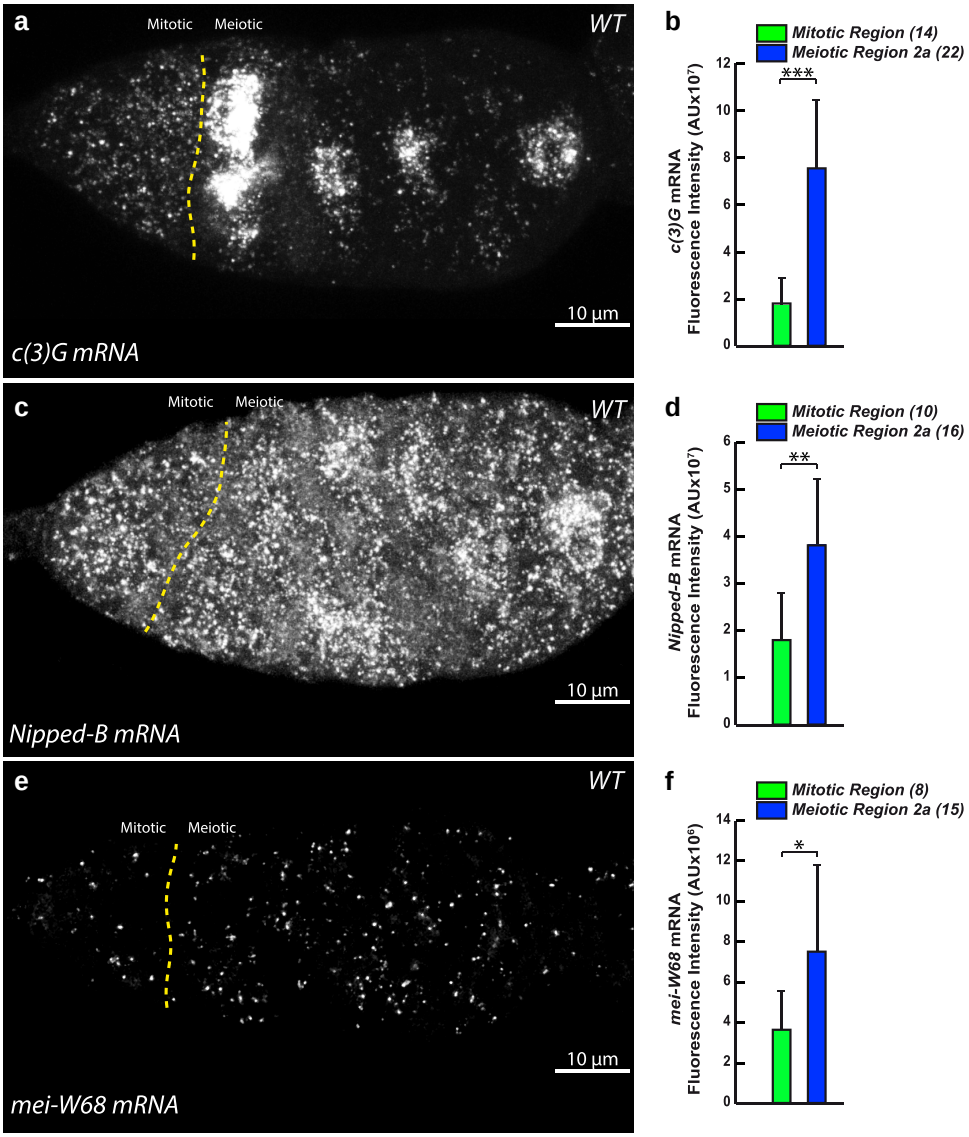

Fig. 2. *C(3)G*, *Nipped-B*, and *mei-W68* meiotic genes mRNA are detected in the mitotic region and their levels increase in the meiotic region. a) Confocal Z-section projection of a wild-type (*WT*) germarium labeled for *c(3)G* mRNA by HCR in situ hybridization. The dashed line delimits the boundary of mitotic and meiotic regions. Scale bar: 10 µm. b) Graph plots of *c(3)G mRNA* fluorescence intensity in mitotic and meiotic 2a regions. ***$P \leq 0.001$ (Mann–Whitney *U*-test). c) Confocal Z-section projection of a *WT* germarium labeled for *Nipped-B* mRNA by HCR in situ hybridization. The dashed line delimits the boundary of mitotic and meiotic regions. Scale bar: 10 µm. d) Graph plots of *Nipped-B mRNA* fluorescence intensity in mitotic and meiotic 2a regions. **$P \leq 0.01$ (Mann–Whitney *U*-test). e) Confocal Z-section projection of a *WT* germarium labeled for *mei-W68* mRNA by HCR in situ hybridization. The dashed line delimits the boundary of mitotic and meiotic 2a regions. Scale bar: 10 µm. f) Graph plots of *mei-W68 mRNA* fluorescence intensity in mitotic and meiotic regions. *$P \leq 0.05$ (Mann–Whitney *U*-test). (*n*) is the number of germaria analyzed for each probe.

both samples, our control experiments demonstrated that we were able to separate germline mitotic cells from meiotic cells and that our results were consistent with previously published data.

We then took advantage of these transcriptome data sets to focus on genes required for the initial stages of meiosis I. We used the single GO term "meiosis I" in Flybase and removed male-specific genes to identify 69 genes. We found that all of these genes were expressed in both mitotic and meiotic cell populations (Fig. 1e; Supplementary Tables 1 and 2). As previously shown by antibody staining, the SC components C(3)G, Corona, and Ord were all found expressed in the mitotic region. We used the DESeq2 package to analyze the differential expression between these genes in the mitotic and meiotic cell populations. Except for a few exceptions, we found that most meiotic genes were expressed at low levels in region 1 and that their expression increases on average by 1.56-fold in region 2 (Fig. 1e; Supplementary Table 1). At one end, *hdm* expression is downregulated 2.3-fold from mitosis to meiosis, almost as strongly as our control gene *bam*, which expression is decreased by 2.7-fold (Fig. 1e; Supplementary Table 1). At the other end, the expression of *cortex* is increased by 4.1-fold. Genes encoding proteins required for homologous recombination such as *mei-W68* and *mei-P22* were among the least expressed in both cell types; nevertheless, their expression increased by 1.5- and 1.6-fold, respectively, in region 2.

To further validate our results, we performed a highly sensitive in situ hybridization (FISH) using the hybridization chain reaction (HCR) method for *C(3)G*, *Nipped-B*, and *mei-W68* RNAs (Choi *et al.* 2018). To unambiguously distinguish the different stages within the mitotic and meiotic regions (Fig. 2, dashed line), we labeled the fusome with an antibody against α-Spectrin (Supplementary Fig.

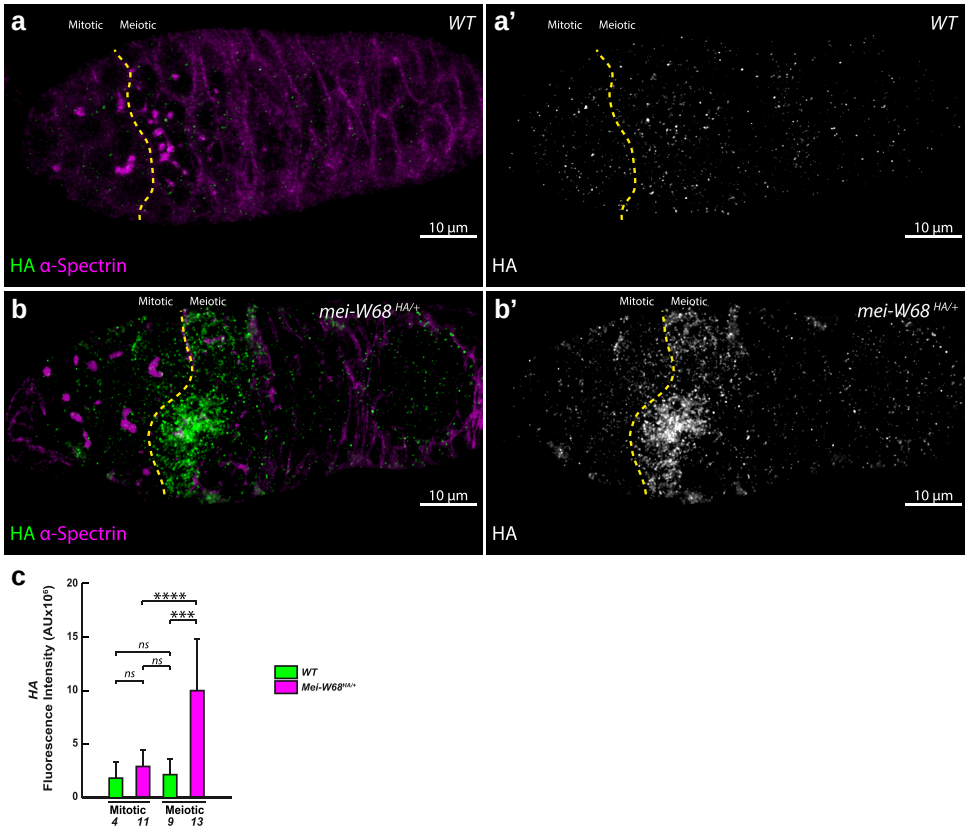

Fig. 3. Mei-W68 protein is only detected in the meiotic region. a and a′) Confocal Z-section projection of a wild-type (*WT*) germarium immunostained for HA and the fusome. The dashed line delimits the boundary of mitotic and meiotic regions. Scale bar: 10 µm. b and b′) Confocal Z-section projection of a *mei-W68*^{HA}/+ germarium immunostained for HA and the fusome. The dashed line delimits the boundary of mitotic and meiotic regions. Scale bar: 10 µm. Note that HA immunostaining is barely detectable in both regions a and a′) of *WT*, while HA is clearly confined to the meiotic region of *W68*^{HA}/+ (compare mitotic and meiotic region in b and b′). c) Graph plots of HA fluorescence intensity in mitotic and meiotic regions. $^{ns}P \geq 0.05$, $^{***}P \leq 0.001$, $^{****}P \leq 0.0001$ (Mann–Whitney *U*-test). Numbers below the bars represent the germaria analyzed.

2a and b). Consistent with our RNAseq data, we found that all 3 genes were expressed in region 1 cells and at very low levels for *mei-W68* and higher levels for *C(3)G* and *Nipped-B* (Fig. 2a, c, and e). Quantification of the fluorescent signals also revealed an increase in RNA levels for all 3 genes as found by the RNAseq analysis (Fig. 2b, d, and f).

Overall, we concluded that we were able to isolate the mitotic germline cells from the meiotic cells and that all meiotic genes started to be expressed in mitotic cells.

mei-W68 gene is expressed in the mitotic region, but Mei-W68 protein is only detected in meiotic cells

Spo11 and TopoVIBL form a meiosis-specific complex, which is conserved across species. In *Drosophila*, Mei-W68 is the homolog of Spo11, while Mei-P22 is a potential homolog of TopoVIBL (Robert *et al.* 2016; Vrielynck *et al.* 2016). The conserved function of this complex is to generate DSBs to initiate recombination between homologous chromosomes. However, in some species such as mouse, zebrafish, and recently jellyfish, these DSBs are also required for the formation of a SC (Romanienko and Camerini-Otero 2000; Blokhina *et al.* 2019; Munro *et al.* 2023), whereas it is not the case in *C. elegans* and *Drosophila* females (Dernburg *et al.* 1998; McKim *et al.* 1998). Here, we wanted to test whether Mei-W68 played a role in homologous chromosome pairing in region 1 before the initiation of meiotic DSBs.

As shown above using RNAseq and RNA FISH, we found that *mei-W68* mRNA is present at low levels in region 1. Next, we wanted to examine whether Mei-W68 protein was present in region 1. Since there is no antibody against Mei-W68 available in *Drosophila* and that Spo11 homologs are also very hard to detect in other species, we decided to knock in a small 3xHA-6xHis tag by CRISPR-Cas9 at the C-terminus of the endogenous protein (Supplementary Fig. 4c). Despite successful integration, we found that the fusion protein was not functional, as no DSBs could be detected with an anti-γH2Av antibody in mei-W68-HA flies (Supplementary Fig. 5). Furthermore, we found that the frequencies of X and chromosome II nondisjunction were similar in *mei-W68-HA/Df*(BSC782) and *mei-W68*^{1}*/Df*(BSC782) (Supplementary Table 6a and b). However, *mei-W68-HA* RNAs were nonetheless translated as we were able to detect a specific signal in region 2a using an anti-HA antibody (Fig. 3b). Quantification of this signal revealed that the levels of Mei-W68-HA protein in region 1 were at background levels and dramatically increased in meiotic cells (Fig. 3a′, b′, and c). These results showed that Mei-W68 protein is probably not present in region 1 and that *mei-W68* mRNA is translated only in *Drosophila* meiotic cells.

Mei-W68 and Mei-P22 are dispensable for centromere pairing in the mitotic region

The failure to detect Mei-W68 protein in the mitotic region could be due to limitations in our detection methods combined with its low expression levels, as suggested by our transcriptome analysis. We therefore used a functional assay to test for a requirement of

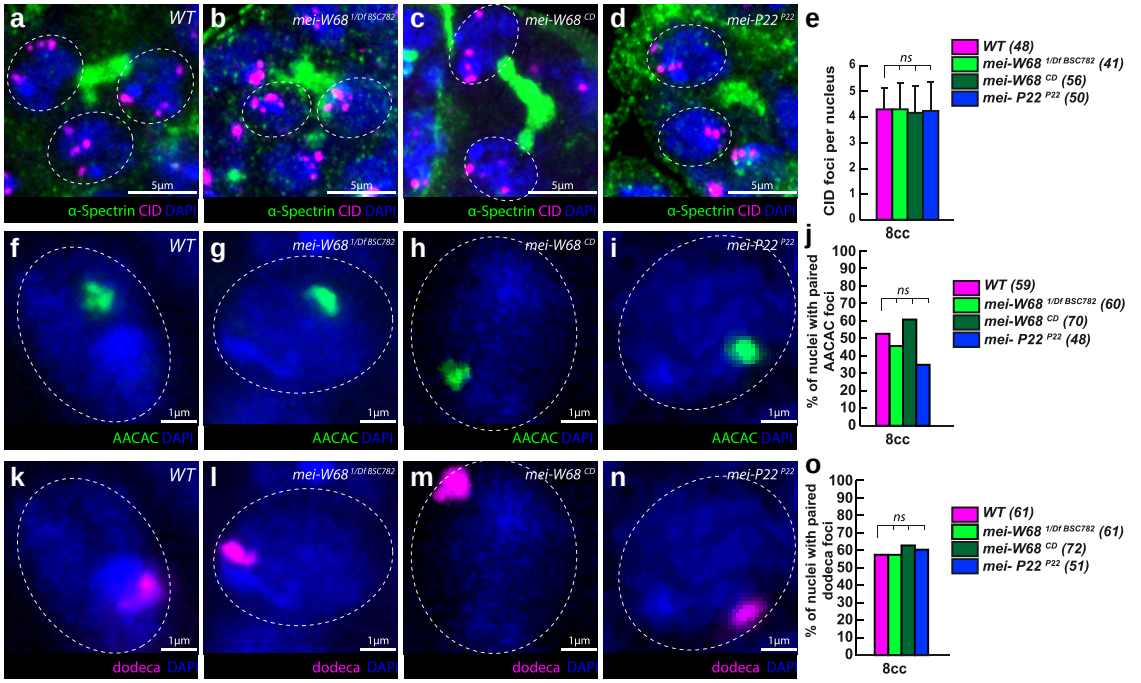

Fig. 4. *mei-W68* and *mei-P22* are dispensable for 8-cell cyst chromosome pairing in females. a–e) Cid pairing in *mei-W68* and *mei-P22* mutant cysts. a–d) Confocal Z-section projections of wild-type (WT), *mei-W68*$^{1/DfBSC782}$, *mei-W68*^{CD}, and *mei-P22*^{P22} 8-cell cysts stained for centromeres (CID), fusome (α-Spectrin), and DNA (DAPI). e) Graph plots of the number of CID foci per nucleus in WT, *mei-W68*$^{1/DfBSC782}$, *mei-W68*^{CD}, and *mei-P22*^{P22} 8-cell cysts. (*n*) is the number of cells analyzed for each genotype. $^{ns}P \geq 0.05$ (2-tailed Student's *t*-test comparing mutants with WT). f–o) Centromeres II and III are paired in the mitotic region of *mei-W68* and *mei-P22* mutant cysts. f–i) Confocal Z-section projections of WT, *mei-W68*$^{1/DfBSC782}$, *mei-W68*^{CD}, and *mei-P22*^{P22} 8-cell cysts labeled with chromosome II centromeric probe (AACAC) and DNA (DAPI). j) Graph plots of the percentage of paired chromosome II centromeres in WT, *mei-W68*$^{1/DfBSC782}$, *mei-W68*^{CD}, and *mei-P22*^{P22} 8-cell cysts. (*n*) is the number of cells analyzed for each genotype. $^{ns}P \geq 0.05$ (χ^2 test comparing mutants with WT). k–n) Confocal Z-section projections of WT, *mei-W68*$^{1/DfBSC782}$, *mei-W68*^{CD}, and *mei-P22*^{P22} 8-cell cysts labeled with chromosome III centromeric probe (dodeca) and DNA (DAPI). Scale bar: 1 µm. o) Graph plots of the percentage of paired chromosome III centromeres in WT, *mei-W68*$^{1/DfBSC782}$, *mei-W68*^{CD2}, and *mei-P22*^{P22} 8-cell cysts. (*n*) is the number of cells analyzed for each genotype. $^{ns}P \geq 0.05$ (χ^2 test comparing mutants with WT). Scale bar: 5 µm in a)–e); 1 µm in f)–o).

Mei-W68 in region 1. In mouse germline cells, Spo11 has been proposed to be required for premeiotic pairing of homologous chromosomes (Boateng *et al.* 2013). We thus assayed whether Mei-W68 was required for premeiotic pairing of centromeres in region 1. To this aim, we used 3 different mutant conditions. Firstly, in *mei-W68*^{1}/*DfBSC782* mutant germaria, there is a 5 kb insertion of a transposable element in the first exon, and there is likely no protein made (McKim and Hayashi-Hagihara 1998) (Supplementary Fig. 4a). Secondly, we replaced by CRISPR-Cas9 the endogenous locus with a form of *mei-W68* mutated in the catalytic domain. Based on sequence alignment of similar constructs in yeast and mouse, we replaced 2 tyrosine (Y80 and Y81) by two phenylalanine in the catalytic domain (*mei-W68*^{CD}; Supplementary Fig. 4b) (Diaz *et al.* 2002; Boateng *et al.* 2013). In this mutant background (*mei-W68*^{1}/*DfBSC782* and *mei-W68*^{CD}), no DSBs could be detected with an anti-γH2Av antibody (Supplementary Fig. 6a–c). Furthermore, we found high levels of nondisjunction for both the X and second chromosomes (Supplementary Table 6a and 6b), indicating that *mei-W68*^{CD} is a strong mutant allele of *mei-W68*. Thirdly, we used a *mei-P22*^{P22} mutant allele and confirmed that DSBs were also completely absent (Supplementary Fig. 6d).

In previous studies, we observed that centromere pairing became prominent in 8-cell germline cysts (Christophorou *et al.* 2013). *Drosophila* diploid cells have 4 pairs of homologous chromosomes, resulting in 8 chromosomes per cell. When all homologs are paired, we can observe 4 distinct dots of CID corresponding to centromere pairing (Takeo *et al.* 2011; Tanneti *et al.* 2011). However, when centromeres are not all paired, we can count more than 4 dots. In the nuclei of *mei-W68*$^{1/DfBSC782}$, *mei-W68*^{CD}, and *mei-P22*^{P22} 8-cell cysts, we counted an average of 4.2, 4.4 and 4.2 ± 0.9–1.1, respectively, of CID foci as compared to 4.2 ± 0.9 in the wild type (Fig. 4a–e), indicating that most chromosomes were paired at their centromeres in these 3 independent mutant conditions compared to wild-type germaria (2-tailed Student's *t*-test; $P = 1$ for *mei-W68*$^{1/DfBSC782}$; $P = 0.7$ for *mei-W68*^{CD}; and $P = 0.8$ for *mei-P22*^{P22}).

We also examined the pairing behavior of individual chromosomes in order to determine if premeiotic centromere pairing occurred between homologous chromosomes. To label the pericentromeric regions of chromosomes II and III, we used the AACAC and dodeca probes, respectively (Joyce *et al.* 2012). To visualize pairing, we performed fluorescence in situ hybridization (DNA FISH) in combination with immunostaining against the fusome marker, α-Spectrin (Fig. 4f–o). We defined chromosomes as paired when only 1 focus was detected or when 2 foci were detected with a separation distance of less than or equal to 0.70 µm (Gong *et al.* 2005; Blumenstiel *et al.* 2008). We found that in *mei-W68*$^{1/DfBSC782}$, *mei-W68*^{CD}, and *mei-P22*^{P22} mutant 8-cell cysts, the number of paired chromosome II at the level of the centromeric regions varies from 52.5% (WT) to 46.7% (*mei-W68*$^{1/DfBSC782}$; χ^2, $P = 0.5$), 61.4% (*mei-W68*^{CD}; χ^2, $P = 0.3$), and 35.4% (*mei-P22*^{P22}; χ^2, $P = 0.07$) (Fig. 4f–j); and for chromosome III, pairing varies from 57.4% (WT) to 57.4% (*mei-W68*$^{1/DfBSC782}$; χ^2, $P = 1$), 64.4% (*mei-W68*^{CD}; χ^2, $P = 0.4$), and 60.8% (*mei-P22*^{P22}; χ^2, $P = 0.7$) (Fig. 4k–o). These results indicate that homologous chromosomes II and III were paired at their centromeres in all mutant conditions similarly to the wild-type condition.

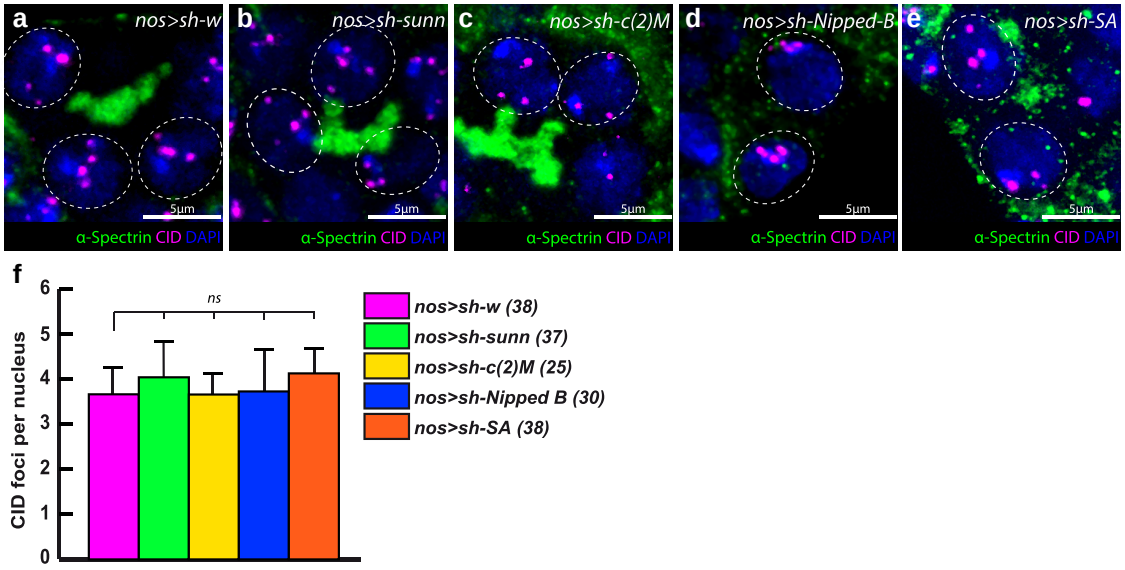

Fig. 5. *Sunn, c(2)M, Nipped-B, and SA* are dispensable for 8-cell cyst chromosome pairing in females. a–e) Confocal Z-section projections of *nos>sh-w*, *nos>sh-sunn*, *nos>sh-c(2)M*, *nos>sh-Nipped-B*, and *nos>sh-SA* 8-cell cysts stained for centromeres (CID), fusome (α-Spectrin), and DNA (DAPI). f) Graph plots of the number of CID foci per nucleus in *nos>sh-w*, *nos>sh-sunn*, *nos>sh-c(2)M*, *nos>sh-Nipped-B*, and *nos>sh-SA* 8-cell cysts. (*n*) is the number of cells analyzed for each genotype. $^{ns}P \geq 0.05$ (2-tailed Student's *t*-test comparing *nos>sh-sunn*, *nos>sh-c(2)M*, *nos>sh-Nipped-B*, and *nos>sh-SA* with *nos>sh-w*). Scale bar: 5 µm.

From these results, we concluded that Mei-W68 and Mei-P22 are not required for early centromere pairing.

Sunn, C(2)M, Nipped-B, and Stromalin are dispensable for centromere pairing in the mitotic region

We previously showed that SC proteins C(3)G and Corona were expressed and required for centromere pairing in region 1 (Christophorou *et al.* 2013). Here, the RNAseq data indicated that many more SC or chromosome-axis proteins could be present in region 1, such as Sunn, C(2)M, Nipped-B or Stromalin (SA), which are meiotic cohesin or cohesin-associated proteins (Hughes *et al.* 2018). To test whether these genes were required for centromere pairing in region 1, we expressed shRNAs targeting each of these genes in germline cells (Fig. 5). On average, we found that the numbers of centromere foci were similar between control germarium (sh-*white*) and in germarium mutant for *sunn*, *C(2)M*, *Nipped-B*, and *Stromalin*, indicating that these genes are not required for the early pairing and clustering of centromeres (Fig. 5a–f). We further tested the efficiency of these shRNA lines by estimating the frequencies of X chromosome nondisjunction. We found that these lines induced efficiently between 8% and 14% of NDJ (Supplementary Table 7). We concluded that, in contrast to SC proteins (C(3)G, Corona, and Ord), cohesins associated to meiotic chromosomes were not required for centromere pairing. These results further suggest that the nature of these complexes may differ at centromeres, where C(3)G and Corona localize in premeiotic cells, compared to the SC along chromosome arms in later meiotic cells.

DSB activity is not detected in the premeiotic region

We then investigated whether DSBs could be present in region 1 despite the absence of Mei-W68 activity. In the *Drosophila* germline, the first sign of DSBs was described in region 2a using an antibody recognizing the phosphorylated H2A variant, also known as γH2Av (Mehrotra and McKim 2006; Lake *et al.* 2013). To avoid using an antibody, we tested a GFP-tagged RPA transgene to label DSBs. RPA binds and protects single-strand DNA (ssDNA) just after resection of the DSB. It is one of the earliest known events of DSB repair. The coating of ssDNA by RPA is, however, transient as it is replaced by Rad51 filaments for DNA repair. To compare the pattern of DSBs precisely in the premeiotic and meiotic regions, we labeled the germarium with an antibody against α-Spectrin recognizing 8-cc stages and against C(3)G to identify meiotic cells. In meiotic cysts, we selected the 2 pro-oocytes that displayed the brightest SC and counted their RPA::GFP dots in the early and late regions 2a and in region 2b (Huynh and St Johnston 2000; Page and Hawley 2001). In a wild-type germarium because RPA is rapidly replaced by Rad51, the GFP signal is expected to be very rare (Fig. 6). Indeed, in this genetic context (*RpA-70::GFP*), we counted an average of 0 (8-cc), 0.7 (early 2a), 2.2 (late 2a), and 0.4 (region 2b) ± 0.6–1.7 GFP foci (Fig. 6a, a′, c, d, d′, g, and g′; Supplementary Movie 1). Furthermore, we found that most RPA–GFP foci were associated with γH2Av, while the opposite was not (Supplementary Fig. 7a, b, and e), indicating a rapid replacement of RPA at DSB sites.

We then introduced RpA-70 EGFP into a *spn-D* mutant background (*RpA-70::GFP, spn-D*^{2}). Spn-D is a meiosis-specific Rad51 homolog that is involved in removing and replacing RPA for DSB repair in germline cells (Abdu *et al.* 2003). In this genetic context, we observed accumulation of GFP dots in the meiotic region (Fig. 6b and b′; Supplementary Movie 2) and not in the mitotic zone, counting an average of 0.2 (8-cc), 19 (early 2a), 16.7 (late 2a), and 19.7 (2b pro-oocytes) ± 0.4–4.4 GFP foci (Fig. 6b, b′, c, e, e′, h, and h′), respectively. We rarely detected RPA::GFP dots in the premeiotic region, indicating that neither Mei-W68 nor other sources induced detectable DSBs in the premeiotic region. In addition, we observed a much greater overlap between RPA and γH2Av dots in the *spn-D* mutant background than in the wild-type condition (Supplementary Fig. 7c–e). This result confirmed the conserved role of Spn-D in RPA replacement during meiotic DSB repair. Finally, in the additional absence of Mei-W68 (*mei-W68*$^{1/DfBSC782}$; *RpA-70::GFP, spn-D*^{2}), we counted 0 (8-cc), 0.2 (early 2a), and 0.3 (late 2a) ± 0.3–0.4 GFP foci (Fig. 6c, f, f′, i,

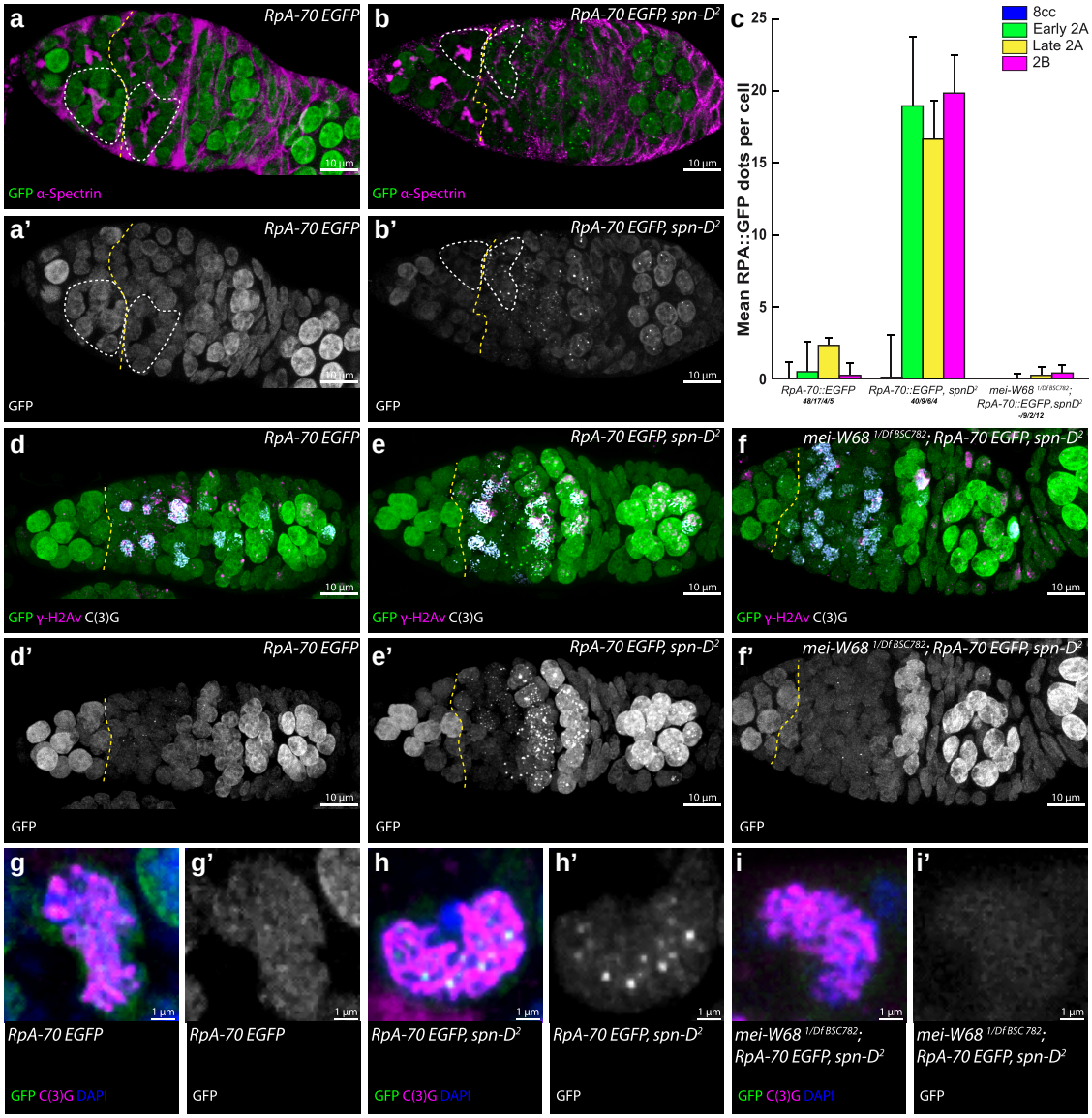

Fig. 6. RpA-70 foci are not detected in the premeiotic region of *Drosophila*. a and a′) Confocal Z-section projection of *RpA-70 EGFP* germarium (a; a′) stained for the fusome (α-Spectrin). Note that RpA-70 EGFP is evenly distributed in the germline nucleoplasm with rare chromatin foci. Scale bar: 10 μm. b and b′) Confocal Z-section projections of *RpA-70 EGFP, spn-D*^{2} germarium (b; b′) stained for the fusome (α-Spectrin). In a *spn-D*^{2} mutant germarium, many RpA-70 EGFP foci are detectable in region 2 and in older egg chambers, here shown in region 3. Scale bar: 10 μm. The dashed line delimits the boundary of mitotic and meiotic regions, with an 8-cell cyst and a 16-cell cyst, respectively, circled by dashed lines. c) Mean number of RpA-70 foci per cell counted in the mitotic 8-cc (staged with α-Spectrin) and meiotic pro-oocytes (staged with C(3)G in early 2A, late 2B, and 2B regions) of *RpA-70 EGFP* control, *RpA-70 EGFP, spn-D*^{2}, and *mei-W68*$^{1/DfBSC782}$*; RpA-70 EGFP, spn-D*^{2}. The number of analyzed cells for each genetic context is labeled as *n/n/n/n*. d–f′) Confocal Z-section projections of *RpA-70 EGFP* (d; d′), *RpA-70 EGFP; spn-D*^{2} (e; e′), and *mei-W68*$^{1/BSC782}$*; RpA-70 EGFP, spn-D*^{2} (f; f′) stained for γ-H2Av and for SC (C(3)G). Note that the number of RpA-70 EGFP foci in region 2 is greatly reduced in *mei-W68*$^{1/BSC782}$*; spn-D*^{2} mutant cells (compare e′ and f′). Scale bar: 10 μm. g–i′) Confocal Z-section projections of selected pro-oocyte nuclei of cysts from *RpA-70 EGFP* (g; g′), *RpA-70 EGFP; spn-D*^{2} (h; h′), and *mei-W68*$^{1/DfBSC782}$*; RpA-70 EGFP, spn-D*^{2} (i; i′) stained for SC (C(3)G) and DNA (DAPI). Scale bar: 1 μm.

and i′), indicating that Mei-W68 is responsible for most RPA dots in a *spn-D* mutant background and, importantly, that its activity is restricted to the meiotic region.

Discussion

In this work, we explored the transcriptome of known meiotic genes at a key transition of germline cell differentiation in *Drosophila* females. For this purpose, we used nonoverlapping mitotic and meiotic cell populations genetically labeled with fluorescence transgenes in an otherwise completely wild-type genetic background. Published methods for separating GSCs and differentiating cysts are based on the enrichment of GSCs in *bam* mutant conditions and on the controlled expression of *bam* (*bam*RNAi; hs-*bam*) to enrich in differentiating cysts (Kai *et al.* 2005; Wilcockson and Ashe 2019; McCarthy *et al.* 2022; Samuels *et al.* 2024). Wild-type ovaries have been used for single-cell technology assigning differentiation stages with known markers to cell clusters (Jevitt *et al.* 2020; Slaidina *et al.* 2021). These methods have provided vast resources for functional analyses. However, they have limitations in resolving with precision the distinct stages of mitosis and meiosis: the first produces mixed population of cysts,

and the second generated very few cell clusters, but has expanded up to 9 distinct states. Our resulting transcriptome data sets reveal that in *Drosophila*, all the genes involved in the first stages of meiosis are already expressed at low levels in the dividing germ cells before they enter the meiotic prophase I. Importantly, we were able to recover from the RNAseq data sets known meiotic genes expressed in the mitotic compartment confirming and extending our previous findings to the whole *Drosophila* genome (Christophorou *et al.* 2013).

Among these genes, we confirmed by in situ hybridization that *mei-W68* is transcribed in the premeiotic region showing increasing levels in the meiotic region. These results are in agreement with the previous single-cell transcriptome data sets in *Drosophila* ovaries, in which germ cells in the germarium were staged using pseudotime analyses (Slaidina *et al.* 2021). Our study also provides new insights into the regulation of *mei-W68* in the germline. We inserted a small HA-His tag at the endogenous C-terminus of Mei-W68, and although this construct is not functional, it allowed us to follow the pattern of *mei-W68* RNA translation. We found that Mei-W68 protein is detected mostly in early region 2a where meiotic DSBs localized and never in region 1. Thus, the primary factors contributing to the presence of Mei-W68 protein in the meiotic region are linked to the regulation of its translation. The importance of translational regulation during germ cell differentiation is well known (Slaidina and Lehmann 2014; Teixeira and Lehmann 2019). Recently, it has been quantified genome wide using Ribo-seq, and this study showed that it is hard to predict the amount of any proteins from the corresponding mRNA levels (Samuels *et al.* 2024). Nonetheless, the presence of meiotic mRNAs in germline mitotic cells may allow a faster transition to meiosis than the activation of meiotic transcription program at the onset of meiosis.

Interestingly, in the mouse, the role of SPO11 in the initiation of pairing was recently challenged. Two independent studies found that early pairing occurred at the premeiotic stage (Boateng *et al.* 2013; Solé *et al.* 2022), while 2 others detected pairing at early leptotene (Ishiguro *et al.* 2014; Scherthan *et al.* 2014); however, they all agreed that early pairing events were independent of DSBs. Moreover, Boateng *et al.* (2013) further showed that pairing was dependent on SPO11 but not of its catalytic activity. On the other hand, 2 independent labs found that SPO11 was not required at all for pairing (Ishiguro *et al.* 2014; Scherthan *et al.* 2014). These conflicting findings led us to ask for the requirement of Mei-W68 in premeiotic pairing in *Drosophila*. Here, we show that neither Mei-W68 nor its putative partner Mei-P22 is involved in centromere pairing in the mitotic region of *Drosophila* females.

We used an Rpa70-GFP reporter as a new read-out of the initiation of meiotic recombination by DSBs (Blythe and Wieschaus 2015). Phosphorylation of the histone variant H2Av (H2AX in mammals) is a widely used mark for DSBs (Madigan *et al.* 2002). We found that in wild-type germarium, the timing and repair of meiotic DSBs reported previously using antibodies against γ-H2Av are in agreement with our results with Rpa70-GFP. RPA foci first appeared in early region 2a, peaked in late region 2a, and then declined in 2b (Mehrotra and McKim 2006; Lake *et al.* 2013). The number of detectable RPA foci at any one time is, however, much smaller than with γ-H2Av, confirming that RPA coating of ssDNA is very transient (Yadav and Bouuaert 2021). In contrast, in mutant conditions where DSBs are stabilized, we counted similar number of foci (19.7 in *spn-D* mutant region 2b) as previously published using antibody staining, 21.2 foci in *spn-D* mutant region 3 (Mehrotra and McKim 2006) and 19.3 foci in *okra* mutant region 2b (Lake *et al.* 2013). As expected, in a *mei-W68* null background, no or few Rpa70-GFP foci were detected as previously reported using the γ-H2Av antibody (Mehrotra and McKim 2006; Lake *et al.* 2013). Importantly, our results with fluorescently labeled Rpa70 confirmed that Mei-W68 does not exhibit early DSB activity in cysts before entering meiosis in region 2. Finally, our results also showed that there are no significant DSBs in the premeiotic region. In dividing embryos, the transient and rapid binding of Rpa70-GFP to sites of replication stress has allowed to measure optically the dynamics of stalled DNA replication during the mitotic cell cycle (Blythe and Wieschaus 2015). Taking advantage of the properties of this reporter, we aim to follow by live imaging the *Drosophila* germarium events of initiation and repair of DSBs in the different genetic contexts.

Data availability

All fly strains are available upon request. Data sets are available from NCBI Sequence Reach Archive (SRA) under BioProject PRJNA1011850 entitled "Isolation of stage-specific germ cells in *Drosophila* germarium". Supplementary Material is available at figshare (https://doi.org/10.25386/genetics.26424277).

Acknowledgments

We are grateful to Shelby Blythe (U. Northwestern), Bloomington Stock Center (NIH P40OD018537), DSHB Hybridoma Center, for the antibodies and flies. We are grateful to the Orion Imaging facility at CIRB (Collège de France).

Funding

JRH lab is supported by Centre National de la Recherche Scientifique (CNRS), Institut National de la Santé et de la Recherche Scientifique (INSERM), Collège de France, Fondation pour la Recherche Médicale (FRM) (Equipe FRM DEQ20160334884); Agence National de la Recherche (ANR) (ANR-20-CE12-, BioPic); and Fondation Bettencourt Schueller (FBS).

Conflicts of interest

The authors declare no conflicts of interest.

Literature cited

Abdu U, Gonzalez-Reyes A, Ghabrial A, Schupbach T. 2003. The *Drosophila* spn-D gene encodes a RAD51C-like protein that is required exclusively during meiosis. Genetics. 165(1):197–204. doi:10.1093/genetics/165.1.197.

Bhalla N, Dernburg AF. 2008. Prelude to a division. Annu Rev Cell Dev Biol. 24(1):397–424. doi:10.1146/annurev.cellbio.23.090506.123245.

Blokhina YP, Nguyen AD, Draper BW, Burgess SM. 2019. The telomere bouquet is a hub where meiotic double-strand breaks, synapsis, and stable homolog juxtaposition are coordinated in the zebrafish, *Danio rerio*. PLoS Genet. 15(1):e1007730. doi:10.1371/journal.pgen.1007730.

Blumenstiel JP, Fu R, Theurkauf WE, Hawley SR. 2008. Components of the RNAi machinery that mediate long-distance chromosomal associations are dispensable for meiotic and early somatic homolog pairing in *Drosophila melanogaster*. Genetics. 180(3):1355–1365. doi:10.1534/genetics.108.092650.

Blythe SA, Wieschaus EF. 2015. Zygotic genome activation triggers the DNA replication checkpoint at the midblastula transition. Cell. 160(6):1169–1181. doi:10.1016/j.cell.2015.01.050.

Boateng KA, Bellani MA, Gregoretti IV, Pratto F, Camerini-Otero RD. 2013. Homologous pairing preceding SPO11-mediated double-strand breaks in mice. Dev Cell. 24(2):196–205. doi:10.1016/j.devcel.2012.12.002.

Cahoon CK, Hawley RS. 2013. Flies get a head start on meiosis. PLoS Genet. 9(12):e1004051. doi:10.1371/journal.pgen.1004051.

Cahoon CK, Hawley RS. 2016. Regulating the construction and demolition of the synaptonemal complex. Nat Struct Mol Biol. 23(5):369–377. doi:10.1038/nsmb.3208.

Carpenter AT. 1975. Electron microscopy of meiosis in *Drosophila melanogaster* females. I. Structure, arrangement, and temporal change of the synaptonemal complex in wild-type. Chromosoma. 51(2):157–182. doi:10.1007/BF00319833.

Chen D, McKearin DM. 2003. A discrete transcriptional silencer in the bam gene determines asymmetric division of the *Drosophila* germline stem cell. Development. 130(6):1159–1170. doi:10.1242/dev.00325.

Choi HMT, Schwarzkopf M, Fornace ME, Acharya A, Artavanis G, Stegmaier J, Cunha A, Pierce NA. 2018. Third-generation in situ hybridization chain reaction: multiplexed, quantitative, sensitive, versatile, robust. Development. 145(12):dev165753. doi:10.1242/dev.165753.

Christophorou N, Rubin T, Bonnet I, Piolot T, Arnaud M, Huynh JR. 2015. Microtubule-driven nuclear rotations promote meiotic chromosome dynamics. Nat Cell Biol. 17(11):1388–1400. doi:10.1038/ncb3249.

Christophorou N, Rubin T, Huynh JR. 2013. Synaptonemal complex components promote centromere pairing in pre-meiotic germ cells. PLoS Genet. 9(12):e1004012. doi:10.1371/journal.pgen.1004012.

Cinalli RM, Rangan P, Lehmann R. 2008. Germ cells are forever. Cell. 132(4):559–562. doi:10.1016/j.cell.2008.02.003.

Crittenden SL, Byrd DT, Kimble J. 2006. Cellular analyses of the mitotic region in the *Caenorhabditis elegans* adult germ line. Mol Biol Cell. 17(7):3051–3061. doi:10.1091/mbc.e06-03-0170.

de Cuevas M, Spradling AC. 1998. Morphogenesis of the *Drosophila fusome* and its implications for oocyte specification. Development. 125(15):2781–2789. doi:10.1242/dev.125.15.2781.

de Massy B. 2013. Initiation of meiotic recombination: how and where? Conservation and specificities among eukaryotes. Annu Rev Genet. 47(1):563–599. doi:10.1146/annurev-genet-110711-155423.

Dernburg AF, McDonald K, Moulder G, Barstead R, Dresser M, Villeneuve AM. 1998. Meiotic recombination in *C. elegans* initiates by a conserved mechanism and is dispensable for homologous chromosome synapsis. Cell. 94(3):387–398. doi:10.1016/S0092-8674(00)81481-6.

Diaz RL, Alcid AD, Berger JM, Keeney S. 2002. Identification of residues in yeast Spo11p critical for meiotic DNA double-strand break formation. Mol Cell Biol. 22(4):1106–1115. doi:10.1128/MCB.22.4.1106-1115.2002.

Dufourt J, Dennis C, Boivin A, Gueguen N, Théron E, Goriaux C, Pouchin P, Ronsseray S, Brasset E, Vaury C. 2014. Spatio-temporal requirements for transposable element piRNA-mediated silencing during *Drosophila oogenesis*. Nucleic Acids Res. 42(4):2512–2524. doi:10.1093/nar/gkt1184.

Evans E, Hogarth C, Mitchell D, Griswold M. 2014. Riding the spermatogenic wave: profiling gene expression within neonatal germ and sertoli cells during a synchronized initial wave of spermatogenesis in mice. Biol Reprod. 90(5):108. doi:10.1095/biolreprod.114.118034.

Fang K, Li Q, Wei Y, Zhou C, Guo W, Shen J, Wu R, Ying W, Yu L, Zi J, *et al.* 2021. Prediction and validation of mouse meiosis-essential genes based on spermatogenesis proteome dynamics. Mol Cell Proteomics. 20:100014. doi:10.1074/mcp.RA120.002081.

Fichelson P, Moch C, Ivanovitch K, Martin C, Sidor CM, Lepesant J-A, Bellaiche Y, Huynh J-R. 2009. Live-imaging of single stem cells within their niche reveals that a U3snoRNP component segregates asymmetrically and is required for self-renewal in Drosophila. Nat Cell Biol. 11(6):685–693. doi:10.1038/ncb1874.

Gong WJ, MicKim KS, Hawley RS. 2005. All paired up with no place to go: pairing, synapsis, and DSB formation in a balancer heterozygote. PLoS Genet. 1(5):e67. doi:10.1371/journal.pgen.0010067.

Gyuricza MR, Manheimer KB, Apte V, Krishnan B, Joyce EF, McKee BD, McKim KS. 2016. Dynamic and stable cohesins regulate synaptonemal complex assembly and chromosome segregation. Curr Biol. 26(13):1688–1698. doi:10.1016/j.cub.2016.05.006.

Hughes SE, Miller DE, Miller AL, Hawley RS. 2018. Female meiosis: synapsis, recombination, and segregation in *Drosophila melanogaster*. Genetics. 208(3):875–908. doi:10.1534/genetics.117.300081.

Huynh JR, St Johnston D. 2000. The role of BicD, Egl, Orb and the microtubules in the restriction of meiosis to the *Drosophila oocyte*. Development. 127(13):2785–2794. doi:10.1242/dev.127.13.2785.

Huynh JR, St Johnston D. 2004. The origin of asymmetry: early polarisation of the Drosophila germline cyst and oocyte. Curr Biol. 14(11):R438–R449. doi:10.1016/j.cub.2004.05.040.

Ishiguro K-I, Kim J, Shibuya H, Hernández-Hernández A, Suzuki A, Fukagawa T, Shioi G, Kiyonari H, Li XC, Schimenti J, *et al.* 2014. Meiosis-specific cohesin mediates homolog recognition in mouse spermatocytes. Genes Dev. 28(6):594–607. doi:10.1101/gad.237313.113.

Jevitt A, Chatterjee D, Xie G, Wang X-F, Otwell T, Huang Y-C, Deng W-M. 2020. A single-cell atlas of adult Drosophila ovary identifies transcriptional programs and somatic cell lineage regulating oogenesis. PLoS Biol. 18(4):e3000538. doi:10.1371/journal.pbio.3000538.

Joyce EF, Apostolopoulos N, Beliveau BJ, Wu CT. 2013. Germline progenitors escape the widespread phenomenon of homolog pairing during *Drosophila* development. PLoS Genet. 9(12):e1004013. doi:10.1371/journal.pgen.1004013.

Joyce EF, Williams BR, Xie T, Wu CT. 2012. Identification of genes that promote or antagonize somatic homolog pairing using a high-throughput FISH-based screen. PLoS Genet. 8(5):e1002667. doi:10.1371/journal.pgen.1002667.

Kai T, Williams D, Spradling AC. 2005. The expression profile of purified *Drosophila* germline stem cells. Dev Biol. 283(2):486–502. doi:10.1016/j.ydbio.2005.04.018.

Keeney S, Giroux CN, Kleckner N. 1997. Meiosis-specific DNA double-strand breaks are catalyzed by Spo11, a member of a widely conserved protein family. Cell. 88(3):375–384. doi:10.1016/S0092-8674(00)81876-0.

Kim HJ, Liu C, Dernburg AF. 2022. How and why chromosomes interact with the cytoskeleton during meiosis. Genes (Basel). 13(5):901. doi:10.3390/genes13050901.

Lake CM, Holsclaw JK, Bellendir SP, Sekelsky J, Hawley RS. 2013. The development of a monoclonal antibody recognizing the *Drosophila melanogaster* phosphorylated histone H2A variant (gamma-H2AV). G3 (Bethesda). 3(9):1539–1543. doi:10.1534/g3.113.006833.

Love MI, Huber W, Anders S. 2014. Moderated estimation of fold change and dispersion for RNA-seq data with DESeq2. Genome Biology. 15(12). doi:10.1186/s13059-014-0550-8.

Madigan JP, Chotkowski HL, Glaser RL. 2002. DNA double-strand break-induced phosphorylation of Drosophila histone variant H2Av helps prevent radiation-induced apoptosis. Nucleic Acids Res. 30(17):3698–3705. doi:10.1093/nar/gkf496.

McCarthy A, Sarkar K, Martin ET, Upadhyay M, Jang S, Williams ND, Forni PE, Buszczak M, Rangan P. 2022. Msl3 promotes germline stem cell differentiation in female Drosophila. Development. 149(1):dev199625. doi:10.1242/dev.199625.

McKearin D, Ohlstein B. 1995. A role for the *Drosophila* bag-of-marbles protein in the differentiation of cystoblasts from germline stem cells. Development. 121(9):2937–2947. doi:10.1242/dev.121.9.2937.

McKim KS, Green-Marroquin BL, Sekelsky JJ, Chin G, Steinberg C, Khodosh R, Hawley RS. 1998. Meiotic synapsis in the absence of recombination. Science. 279(5352):876–878. doi:10.1126/science.279.5352.876.

McKim KS, Hayashi-Hagihara A. 1998. mei-W68 in *Drosophila melanogaster* encodes a Spo11 homolog: evidence that the mechanism for initiating meiotic recombination is conserved. Genes Dev. 12(18):2932–2942. doi:10.1101/gad.12.18.2932.

Mehrotra S, McKim KS. 2006. Temporal analysis of meiotic DNA double-strand break formation and repair in *Drosophila* females. PLoS Genet. 2(11):e200. doi:10.1371/journal.pgen.0020200.

Munro C, Cadis H, Pagnotta S, Houliston E, Huynh JR. 2023. Conserved meiotic mechanisms in the cnidarian *Clytia hemisphaerica* revealed by Spo11 knockout. Sci Adv. 9(4):eadd2873. doi:10.1126/sciadv.add2873.

Page SL, Hawley RS. 2001. C(3)G encodes a *Drosophila* synaptonemal complex protein. Genes Dev. 15(23):3130–3143. doi:10.1101/gad.935001.

Pasierbek P, Jantsch M, Melcher M, Schleiffer A, Schweizer D, Loidl J. 2001. A *Caenorhabditis elegans* cohesion protein with functions in meiotic chromosome pairing and disjunction. Genes Dev. 15(11):1349–1360. doi:10.1101/gad.192701.

Robert T, Nore A, Brun C, Maffre C, Crimi B, Guichard V, Bourbon H-M, de Massy B. 2016. The TopoVIB-like protein family is required for meiotic DNA double-strand break formation. Science. 351(6276):943–949. doi:10.1126/science.aad5309.

Rohozkova J, Hulkova L, Fukalova J, Flachs P, Hozak P. 2019. Pairing of homologous chromosomes in *C. elegans* meiosis requires DEB-1—an orthologue of mammalian vinculin. Nucleus. 10(1):93–115. doi:10.1080/19491034.2019.1602337.

Romanienko PJ, Camerini-Otero RD. 1999. Cloning, characterization, and localization of mouse and human SPO11. Genomics. 61(2):156–169. doi:10.1006/geno.1999.5955.

Romanienko PJ, Camerini-Otero RD. 2000. The mouse Spo11 gene is required for meiotic chromosome synapsis. Mol Cell. 6(5):975–987. doi:10.1016/S1097-2765(00)00097-6.

Rubin T, Macaisne N, Huynh JR. 2020. Mixing and matching chromosomes during female meiosis. Cells. 9(3):696. doi:10.3390/cells9030696.

Rubin T, Macaisne N, Vallés AM, Guilleman C, Gaugué I, Dal Toe L, Huynh JR. 2022. Premeiotic pairing of homologous chromosomes during *Drosophila* male meiosis. Proc Natl Acad Sci U S A. 119(47):e2207660119. doi:10.1073/pnas.2207660119.

Samuels TJ, Gui J, Gebert D, Karam Teixeira F. 2024. Two distinct waves of transcriptome and translatome changes drive *Drosophila* germline stem cell differentiation. EMBO J. 43(8):1591–1617. doi:10.1038/s44318-024-00070-z.

Scherthan H, Schofisch K, Dell T, Illner D. 2014. Contrasting behavior of heterochromatic and euchromatic chromosome portions and pericentric genome separation in pre-bouquet spermatocytes of hybrid mice. Chromosoma. 123(6):609–624. doi:10.1007/s00412-014-0479-4.

Schmittgen TD, Livak KJ. 2008. Analyzing real-time PCR data by the comparative CT method. Nature Protocols. 3(6):1101–1108. doi:10.1038/nprot.2008.73.

Slaidina M, Gupta S, Banisch TU, Lehmann R. 2021. A single-cell atlas reveals unanticipated cell type complexity in *Drosophila* ovaries. Genome Res. 31(10):1938–1951. doi:10.1101/gr.274340.120.

Slaidina M, Lehmann R. 2014. Translational control in germline stem cell development. J Cell Biol. 207(1):13–21. doi:10.1083/jcb.201407102.

Solé M, Blanco J, Gil D, Valero O, Cárdenas B, Fonseka G, Anton E, Pascual Á, Frodsham R, Vidal F, *et al.* 2022. Time to match; when do homologous chromosomes become closer? Chromosoma. 131(4):193–205. doi:10.1007/s00412-022-00777-0.

Spradling AC. 1993. Developmental genetics of oogenesis. In: BateM, Martinez Arias A, editors. Development of Drosophila melanogaster. Plainview, New York: Cold Spring Harbor Press. p. 1–70.

Takeo S, Lake CM, Morais-de-Sa E, Sunkel CE, Hawley RS. 2011. Synaptonemal complex-dependent centromeric clustering and the initiation of synapsis in *Drosophila* oocytes. Curr Biol. 21(21):1845–1851. doi:10.1016/j.cub.2011.09.044.

Tanneti NS, Landy K, Joyce EF, McKim KS. 2011. A pathway for synapsis initiation during zygotene in *Drosophila* oocytes. Curr Biol. 21(21):1852–1857. doi:10.1016/j.cub.2011.10.005.

Teixeira FK, Lehmann R. 2019. Translational control during developmental transitions. Cold Spring Harb Perspect Biol. 11(6):a032987. doi:10.1101/cshperspect.a032987.

Tsubouchi T, Roeder GS. 2005. A synaptonemal complex protein promotes homology-independent centromere coupling. Science. 308(5723):870–873. doi:10.1126/science.1108283.

Vallés AM, Huynh JR. 2020. Isolation of stage-specific germ cells using FACS in *Drosophila germarium*. Methods Cell Biol. 158:11–24. doi:10.1016/bs.mcb.2020.02.003.

Vrielynck N, Chambon A, Vezon D, Pereira L, Chelysheva L, De Muyt A, Mézard C, Mayer C, Grelon M. 2016. A DNA topoisomerase VI–like complex initiates meiotic recombination. Science. 351(6276):939–941. doi:10.1126/science.aad5196.

Wang PJ, McCarrey JR, Yang F, Page DC. 2001. An abundance of X-linked genes expressed in spermatogonia. Nat Genet. 27(4):422–426. doi:10.1038/86927.

Wilcockson SG, Ashe HL. 2019. Drosophila ovarian germline stem cell cytocensor projections dynamically receive and attenuate BMP signaling. Dev Cell. 50(3):296–312.e5. doi:10.1016/j.devcel.2019.05.020.

Yadav VK, Bouuaert CC. 2021. Mechanism and control of meiotic DNA double-strand break formation in *S. cerevisiae*. Front Cell Dev Biol. 9:642737. doi:10.3389/fcell.2021.642737.

Zheng Y, Zhang L, Jin L, Zhang P, Li F, Guo M, Gao Q, Zeng Y, Li M, Zeng W. 2022. Unraveling three-dimensional chromatin structural dynamics during spermatogonial differentiation. J Biol Chem. 298(2):101559. doi:10.1016/j.jbc.2021.101559.

Zickler D, Kleckner N. 2015. Recombination, pairing, and synapsis of homologs during meiosis. Cold Spring Harb Perspect Biol. 7(6):a016626. doi:10.1101/cshperspect.a016626.

Editor: P. Geyer